TÜBİTAK

Turkish Journal of Earth Sciences

http://journals.tubitak.gov.tr/earth/

Research Article

Turkish J Earth Sci
(2013) 22: 778-792

doi:10.3906/yer-1207-2

# Paleomagnetic rotations in the Late Miocene sequence from the Çankırı Basin (Central Anatolia, Turkey): the role of strike-slip tectonics

**Stella LUCIFORA[1], Francesca CIFELLI[1,*], F. Bora ROJAY[2], Massimo MATTEI[1]**

[1]Department of Sciences, Roma Tre University, Largo San Leonardo Murialdo 1, 00146 Rome, Italy
[2]Department of Geological Engineering, Middle East Technical University, 06531 Ankara, Turkey

**Received:** 10.07.2012 • **Accepted:** 29.11.2012 • **Published Online:** 26.08.2013 • **Printed:** 25.09.2013

**Abstract:** In this paper, new paleomagnetic and anisotropy of magnetic susceptibility (AMS) data from Miocene continental units of the Çankırı Basin are presented, with the main goal of providing additional constraints on its deformational and rotational history during the Late Cenozoic. AMS data indicate a tectonic origin for the magnetic fabric, suggesting that Upper Miocene units were still involved in the deformation processes. Paleomagnetic data show that tectonic rotations in the Çankırı Basin do not show a symmetrical distribution along the opposite edges of the basin, as expected from the observed Ω-shape. In particular, by combining our data with those already published, we observe that tectonic rotations increase from the southern portion of the basin toward the north and from the central part toward the basin margins. This distribution reasonably matches with a post-Late Miocene reactivation of the Çankırı Basin margin fault systems, possibly related to the activity of the right-lateral North Anatolian strike-slip fault. In this tectonic interpretation, the complex pattern of paleomagnetic rotations appears to be connected with a local block rotation mechanism due to the activity of faults with strike-slip components of motion along the tectonic margins of the Çankırı Basin.

**Key words:** Paleomagnetic rotations, oroclinal bending, Central Anatolia, Neogene, strike-slip tectonics

## 1. Introduction

In the last few decades, a large number of paleomagnetic studies have been carried out in Turkey, with the aim of defining the northward latitudinal drift of the different microcontinents now amalgamated in the Anatolian region (e.g., Van Der Voo 1968; Sanver & Ponat 1981; Evans & Hall 1990; Morris & Robertson 1993) and to shed light on the role of crustal block rotations along the North Anatolian Fault Zone and within the Anatolian Block (e.g., Saribudak *et al.* 1990; Platzman *et al.* 1994; Michel *et al.* 1995; Tatar *et al.* 1995; Piper *et al.* 1996; Gürsoy *et al.* 1997; Piper *et al.* 1997; Platzman *et al.* 1998, Piper *et al.* 2010). The role of paleomagnetic rotations in the origin and tectonic evolution of curved tectonic structures and sedimentary basins has been partially investigated in Central and Northern Turkey. Meijers *et al.* (2010) suggested that the curved shape of the central Pontides orogenic belt resulted from oroclinal bending during the latest Cretaceous to earliest Paleocene times, whereas Kaymakçı *et al.* (2003), on the basis of structural and paleomagnetic data, suggested that the Ω-shape of the Çankırı Basin (Central Anatolia) resulted from opposite rotations along the basin margins, related to the indentation of the Kirşehir Block against the Sakarya continent. Also from this evidence, Mejiers *et al.* (2010) proposed an overall tectonic model for the evolution of Central and North Turkey and suggested that deformation was localized in the northern part of the central Pontides during Late Cretaceous-Tertiary convergence between the different Anatolian blocks, resulting in oroclinal bending lasting until the Paleocene. After that period, deformation was mainly expressed by thin-skin thrust tectonics, which propagated southwards and were concentrated in the Çankırı Basin, thus causing the present-day curved shape.

In this work, we present new paleomagnetic and anisotropy of magnetic susceptibility (AMS) data from Miocene continental units from the Çankırı Basin, with the main objective of further constraining the time and spatial distribution of tectonic rotations during Late Cenozoic times. In particular, AMS and paleomagnetic measurements on the rock collection from the Çankırı Basin were carried out with a 2-fold purpose: to define the timing of rotation in the Late Miocene sediments and give further constraint to the indentation mechanism proposed by Kaymakçı *et al.* (2003); and to determine the fabric of the Miocene sediments and to assess whether they have

* Correspondence: francesca.cifelli@uniroma3.it

a fabric dominated by sedimentary or tectonic processes. Our results show that paleomagnetic rotations in the Çankırı Basin do not have a symmetrical distribution along the opposite edges of the basin and, when considered together with those published by Kaymakçı *et al.* (2003), they do not fit with the indentation model considered to be responsible for the Ω-shape of the Çankırı Basin. We propose that the complex pattern of tectonic rotations measured in the Çankırı Basin is due to strike-slip motion along the basin margins, related to activity on the North Anatolian Fault.

## 2. Geological setting of the Çankırı Basin

The Çankırı Basin is an important tectonic feature for understanding the tectonic history of Central Anatolia, due to its tectonic position at the contact between the Pontides and the Anatolide-Tauride Block (Figure 1a, b). The tectono-sedimentary evolution of the Central Anatolia basins has been mainly controlled by the progressive closure of the northern Neotethys Ocean, and then by the initiation and subsequent deformation on the North Anatolian Fault activity (Şengör & Yılmaz 1981). During the Late Cretaceous-Paleogene, accretionary

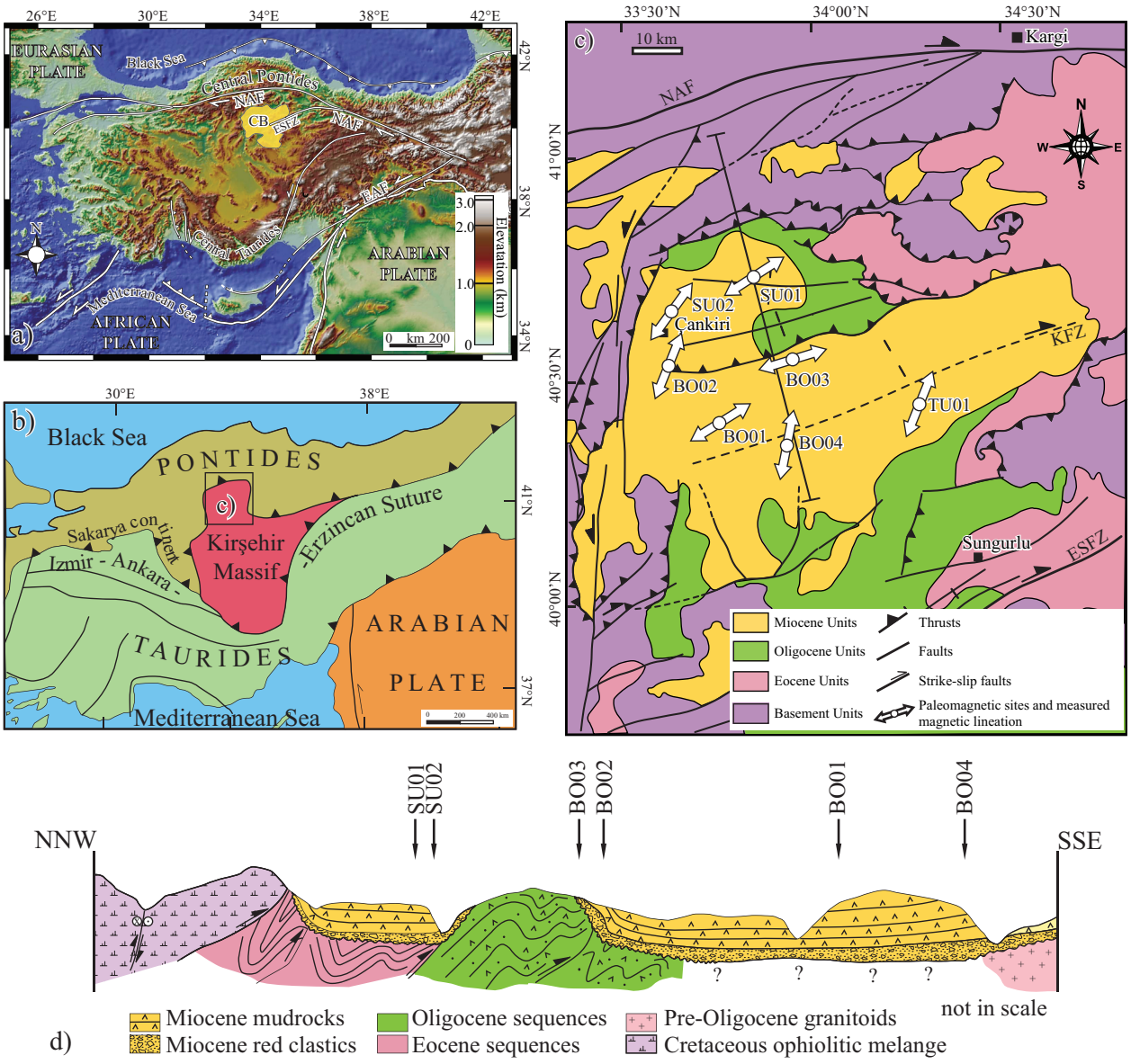


**Figure 1.** Tectonic setting (a) and geological sketch (b) of Eastern Mediterranean area. (c) Geological map of the Çankırı Basin. Sampled sites and magnetic lineations from AMS measurements from this work are shown. (d) Simplified geological section cutting the Çankırı Basin (its trace is indicated in Figure 1c). NAF, North Anatolian Fault; EAF, Eastern Anatolian Fault; CB, Çankırı Basin; KFZ, Kızılırmak Fault zone; ESFZ, Ezinepazarı–Sungurlu Fault zone.

prisms and fore-arc basins developed to be followed in Eocene times by piggyback to peripheral basins (Şengör & Yılmaz 1981; Rojay 1995; Görür *et al.* 1998). After the closure of the northern Neotethys during the Miocene (Gannser 1974; Şengör *et al.* 1981; Kaymakçı 2000; Şengör 2003; Rojay *et al.* 2004), the Central Anatolian region was characterized by the formation of narrow continental basins (e.g., Ankara and Çankırı Basins) and extensive Neogene volcanism (e.g., Galatia and Cappadocia volcanic terrains). According to Kaymakçı *et al.* (2009), the Çankırı Basin first developed as a fore-arc basin from Late Cretaceous to Middle Paleocene times, and then as a foreland basin during the Late Paleocene-Early Miocene, straddling the İzmir-Ankara-Erzincan suture zone (Figure 1b). The Ω-shaped Çankırı Basin is bounded by Cretaceous ophiolitic mélanges at the northern and western edges, by a N–S oriented left-lateral strike-slip fault overprinted on an imbricated accretionary wedge at the western edge, and by the Kırşehir crystalline complex in the south (Figures 1c and 1d). The basin is filled with 4 km of Late Cretaceous to recent deposits, which can be grouped into 5 sedimentary sequences (Kaymakçı 2000). The oldest sedimentary sequence consists of tectonically intercalated Late Cretaceous deep marine sediments alternating with mafic volcanic rocks, volcano-clastic rocks, proximal regressive shallow marine units, and Paleocene littoral red clastic rocks and carbonates, which represent the subduction history of the northern Neotethys in the region. The second sequence is a Late Paleocene to mid-Oligocene, more than 1 km thick, regressive flysch to molasse type of succession intercalated with mafic to intermediate volcanic rocks and nummulitic limestones. The third sequence comprises a very thick (up to 2 km) sequence of Late Eocene to mid-Oligocene continental red clastic rocks and evaporites. The fourth sequence is up to 1 km thick and represented by Early Miocene to Pliocene fluvio-lacustrine deposits. The Late Pliocene-Quaternary alluvial fan deposits and recent alluvium (fifth sequence) locally overlie all these units (Kaymakçı 2000).

The main structures that shape the current geometry of the Çankırı Basin are the thrust and reverse faults delineating its western and northern rims (Figure 1c). A belt of NNE-striking folds defines the eastern margin of the basin. In the south, the basin infill laps onto the basement (Kaymakçı 2000). Other major structures affecting the Çankırı Basin are the right-lateral Kizilirmak Fault zone (KFZ) and Ezinepazarı–Sungurlu Fault zone (ESFZ). These are WSW–ENE oriented and displace the ophiolitic rim, the basement, and the basin infill, which included Late Miocene units indicating a post-Late Miocene tectonic activity (Kaymakçı *et al.* 2003).

## 3. Sampling and methods

For this study, we collected 162 oriented cylindrical samples from 7 sites (Figure 1c; Table 1). All the sampled sites belong to the Miocene continental succession comprising fluvio-lacustrine units, frequently in succession with evaporites. In particular, sites have been collected from the continental Tuğlu, Süleymanlı, and Bozkır Formations (Late Miocene), which lie within the fourth stratigraphic sequence of Kaymakçı (2000). Four sites have been sampled from the Bozkır Formation (MN13–MN15, Messinian-Lower Pliocene) which crops out in the central (BO01, BO03, and BO04) and western parts of the basin (BO02). The sample sites are located on top of a hidden thrust fault, which cuts Oligocene sequences and is sealed by Middle-Late Miocene units (Figure 1d). At site BO02, a 90-m-long stratigraphic section (64 samples) was sampled. This section corresponds to the lower part of the Bozkır Formation, close to the contact with the underlying formation (Süleymanlı Formation). The section is formed

**Table 1.** List of anisotropy factors computed at each site in the Çankırı Basin.

| Site | n/N | $K_m$ | L | F | P' | T | $S_0$ | D, I ($K_{min}$) | D, I ($K_{max}$) | $e_{1,2}$ |
|---|---|---|---|---|---|---|---|---|---|---|
| TU01 | 24/24 | 465 | 1.006 | 1.010 | 1.017 | 0.195 | 40°, 20° | 259, 55 | 22, 21 | 8.0 |
| SU01 | 8/10 | 1265 | 1.003 | 1.014 | 1.019 | 0.569 | variable | 197, 85 | 57, 4 | 34.8 |
| SU02 | 12/12 | 442 | 1.007 | 1.014 | 1.022 | 0.328 | 348°, 10° | 184, 84 | 36, 5 | 9.7 |
| BO01 | 18/18 | 245 | 1.002 | 1.018 | 1.022 | 0.768 | 320°, 10° | 222, 80 | 58, 10 | 27.4 |
| BO02 | 64/64 | 121 | 1.003 | 1.026 | 1.032 | 0.759 | variable | 114, 77 | 22, 0.4 | 29.7 |
| BO03 | 13/13 | 1170 | 1.007 | 1.070 | 1.086 | 0.791 | 178°, 27° | 352, 60 | 253, 5 | 16.8 |
| BO04 | 23/23 | 293 | 1.003 | 1.035 | 1.043 | 0.827 | sub-horiz | 118, 86 | 11, 1 | 44.3 |

n/N = measured/sampled samples; $K_m = (K_{max} + K_{int} + K_{min}) / 3$ (mean susceptibility, in $10^{-6}$ SI units); $L = K_{max} / K_{int}$; $F = K_{int} / K_{min}$; $Pj = \exp \{2[(\eta1 - \eta)^2 + (\eta2 - \eta)^2 + (\eta3 - \eta)^2]\}^{1/2}$ (corrected anisotropy degree; Jelinek, 1981); $Tj = 2(\eta2 - \eta3) / (\eta1 - \eta3) - 1$ (shape factor; Jelinek 1981); $S_0$ = bedding attitude (azimuth of the dip and dip values); $\eta1 = \ln K_{max}$; $\eta2 = \ln K_{int}$; $\eta3 = \ln K_{min}$; $\eta = (\eta1 + \eta2 + \eta3) / 3$; $e_{1-2}$: semiangle of the 95% confidence ellipses around the principal susceptibility axes.

by grayish clays and silty clays interbedded with thick layers of gypsum. Two sites (SU01–SU02) have been sampled in the northwestern part of the basin from the Messinian (MN13) Süleymanlı Formation to the south of a thrust belt where the Cretaceous ophiolitic mélange is thrust onto Eocene and Oligocene red clastics, and Miocene red clastics are steeply tilted (Figure 1d). Finally, a stratigraphic section (TU01) has been sampled in the northeastern part of the basin. The section is composed of fluvio-lacustrine sediments formed by clays and sandy clays intercalated with sandy layers from the Tuğlu Formation (Tortonian, MN9–12).

At each site, cores were drilled with an ASC 280E petrol-powered portable drill and oriented in situ by a magnetic compass, corrected to account for the local magnetic declination according to the NOAA National Geophysical data center. From each core, 1 to 3 standard (25 mm in diameter × 22 mm in height) cylindrical specimens were cut. All magnetic measurements were carried out at the Roma Tre University and Istituto Nazionale di Geofisica e Vulcanologia (INGV, Rome) paleomagnetic laboratories. In order to identify the main magnetic carriers in these sediments, rock magnetic analyses on selected specimens were carried out, which included:

1) The measurement of hysteresis properties using a MicroMag alternating gradient magnetometer (AGM model 2900, Princeton Measurements Corporation) with a maximum applied field of 1 T. From hysteresis cycles, after subtraction of the paramagnetic high-field susceptibility after saturation, we calculated the coercive force ($B_c$), the saturation remnant magnetization ($M_{rs}$), and the saturation magnetization ($M_s$).

(2) Stepwise acquisition of isothermal remanent magnetization (IRM) and subsequent backfield DC demagnetization (both in a succession of fields up to 1 T), measured on the same samples on the Micromag AGM. The coercivity of remanence ($B_{cr}$) was computed from the backfield demagnetization curves.

(3) The measure of the variation of susceptibility with temperature in some representative specimens.

The natural remanent magnetization (NRM) was analyzed using 2G Enterprises DC-SQUIDs cryogenic magnetometers, installed within a magnetically shielded room. The NRM of one specimen per core was measured following progressive stepwise demagnetization using thermal and alternating field (AF) procedures. The thermal demagnetization was carried out using small temperature increments (50 °C up to 300 °C and 30 °C above 300 °C) until the NRM decreased below the limit of the instrument sensitivity or random changes of the paleomagnetic directions were observed. Stepwise AF demagnetization was carried out using a set of 3 orthogonal AF coils mounted inline on the 2G Enterprises system, with steps of 5–10 mT up to 100 mT. The characteristic remanent magnetization (ChRM) was resolved from the orthogonal vector projections and their equivalent directions were calculated by principal component analysis (Kirschvink 1980). For each site, the mean direction was computed using standard analysis (Fisher 1953).

The measurement of the low-field AMS was also carried out. AMS represents a cheap, rapid, and nondestructive technique for the characterization of the mineral fabric of rocks (Hrouda 1982). AMS is defined by a second-rank tensor and approximated geometrically by an ellipsoid with principal axes $K_{max}$, $K_{int}$, $K_{min}$, in which the highest intensity of magnetization is induced along the long axis ($K_{max}$) and the weakest intensity along the short axis ($K_{min}$). A range of parameters has been defined quantifying the magnitude of anisotropy and for defining the shape of the ellipsoid (see Table 1; Jelínek 1981; Hrouda 1982). The magnitude of lineation L of the ellipsoid is defined as $K_{max}/K_{min}$, and the magnetic foliation F is defined by $K_{int}/K_{min}$. The anisotropy degree and the shape parameter are expressed by parameters P' and T, respectively. AniSoft software (Chadima & Jelinek 2009) was used for these calculations.

## 4. Results

### 4.1. AMS results

The distribution of magnetic susceptibility values ($K_m$) indicates a range of 100–500 × $10^{-6}$ SI for the majority of the specimens (Figure 2a). This suggests a significant paramagnetic contribution of the clay matrix to the bulk susceptibility. However, some specimens show higher susceptibility values (up to 2400 × $10^{-6}$ SI in site SU01), suggesting a major ferromagnetic content in these samples. The L parameter ranges between 1.002 and 1.007, whereas the F parameter ranges between 1.01 and 1.07 (Figure 2b; Table 1). P' values are less than 1.1 and T values are all positive (Figure 2c). The shape of the ellipsoid is mainly oblate with a well-developed magnetic foliation recognized by well-grouped $K_{min}$ axes in most cases (Figure 3). The main magnetic susceptibility directions for each site are generally tightly grouped (Figures 3b–3g), with only TU01 characterized by a girdle distribution of $K_{int}$ and $K_{min}$ axes (Figure 3a).

At the site scale, a tectonic control on the magnetic fabric is well recognizable, even when the primary sedimentary fabric is still preserved, as is the case in most of the sites (Figure 3). A well-defined magnetic lineation is defined, which parallels the main structural trends documented in the area (Figure 1c). The central part of the basin is characterized by ENE-WSW trending magnetic lineations, parallel to the main fold axes that characterize this area. In the western border, magnetic

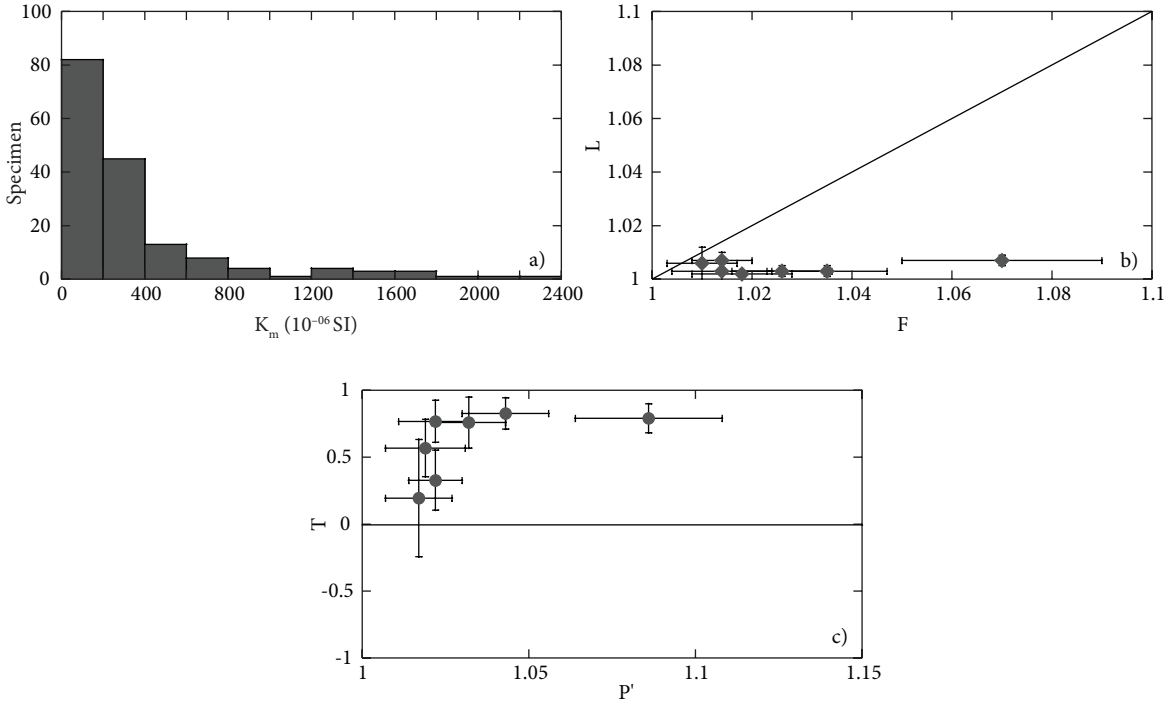


**Figure 2.** Magnetic parameters of analyzed samples in the Çankırı Basin. (a) Frequency distribution of the mean susceptibility ($K_m$) values for the entire set of specimens; (b) site-mean magnetic lineation L vs. site-mean magnetic foliation F diagram; (c) site-mean degree of anisotropy P' vs. shape factor T diagram.

lineations are oriented NNE-SSW and reflect the change in fold axis orientation, which in this area is NNE-SSW. In the eastern part of the basin, magnetic lineation is NNE-SSW–oriented, which is almost parallel to the trend of the thrusts in this area. Collectively, these data suggest that the magnetic fabric developed in a compressional tectonic setting and that magnetic lineations follow the geometry of the main thrust faults in the basin.

### 4.2. Magnetic mineralogy and demagnetization of the NMR

Representative examples of hysteresis loops are shown in Figure 4. Results from these analyses indicate magnetic saturation ($M_s$) values from 0.001 to 0.1 $Am^2/kg$. In some samples, a paramagnetic contribution due to the clay matrix was observed (gray curves in Figures 4a, 4c, and 4d). Figure 4a shows a hysteresis loop weakly developed, indicating the presence of low coercivity minerals, such as magnetite. Figure 4b shows a typical wasp-waisted shape, which suggests the occurrence of a mixture of 2 minerals with different coercitivity values. Loops in Figures 4c and 4d are characterized by a well-developed hysteresis and a more open shape, which suggest the presence of a mineral with higher coercivity, probably hematite. IRM curves (Figure 4e) confirm the presence of ferromagnetic minerals with different coercivity. Some samples (SULE18, SULE31, SULE19, TUGLU10) reach 90% saturation values between 0.2 and 0.3 T, suggesting the dominance of a low coercivity ferromagnetic mineral such as magnetite, whereas other samples (TUGLU32, TUGLU37) do not saturate at 1 T, suggesting the coexistence of low coercitivity (magnetite) and a high coercivity ferromagnetic mineral such as hematite. These results are also confirmed by thermomagnetic analyses, which show a sharp decrease in magnetic susceptibility between 400 and 600 °C, indicative of the presence of magnetite, and a small tail in magnetic susceptibility above this temperature indicating the presence of hematite (Figure 4f).

The intensities of the NRM vary by more than 3 orders of magnitude. In some samples, NRM was found to be too weak to measure accurately (NRM < $10^{-5}$ A/m) or unstable after the first demagnetization steps. These samples were excluded from further paleomagnetic evaluation (Table 2). Most of the samples are characterized by a single component of magnetization with both normal (Figures 5a–5d) and reversed (Figures 5e–5h) polarity. The normal polarity ChRM has been isolated between 180 and 630–670 °C (Figures 5a, 5b, and 5c) or between 10 and 100 mT (Figure 5d), suggesting the presence of both hematite and magnetite. Reversed polarity samples are generally characterized by a normal polarity viscous component, which is completely removed at 180–230 °C (Figure 5f), or at 10 mT (Figure 5g), and by ChRM, which has been

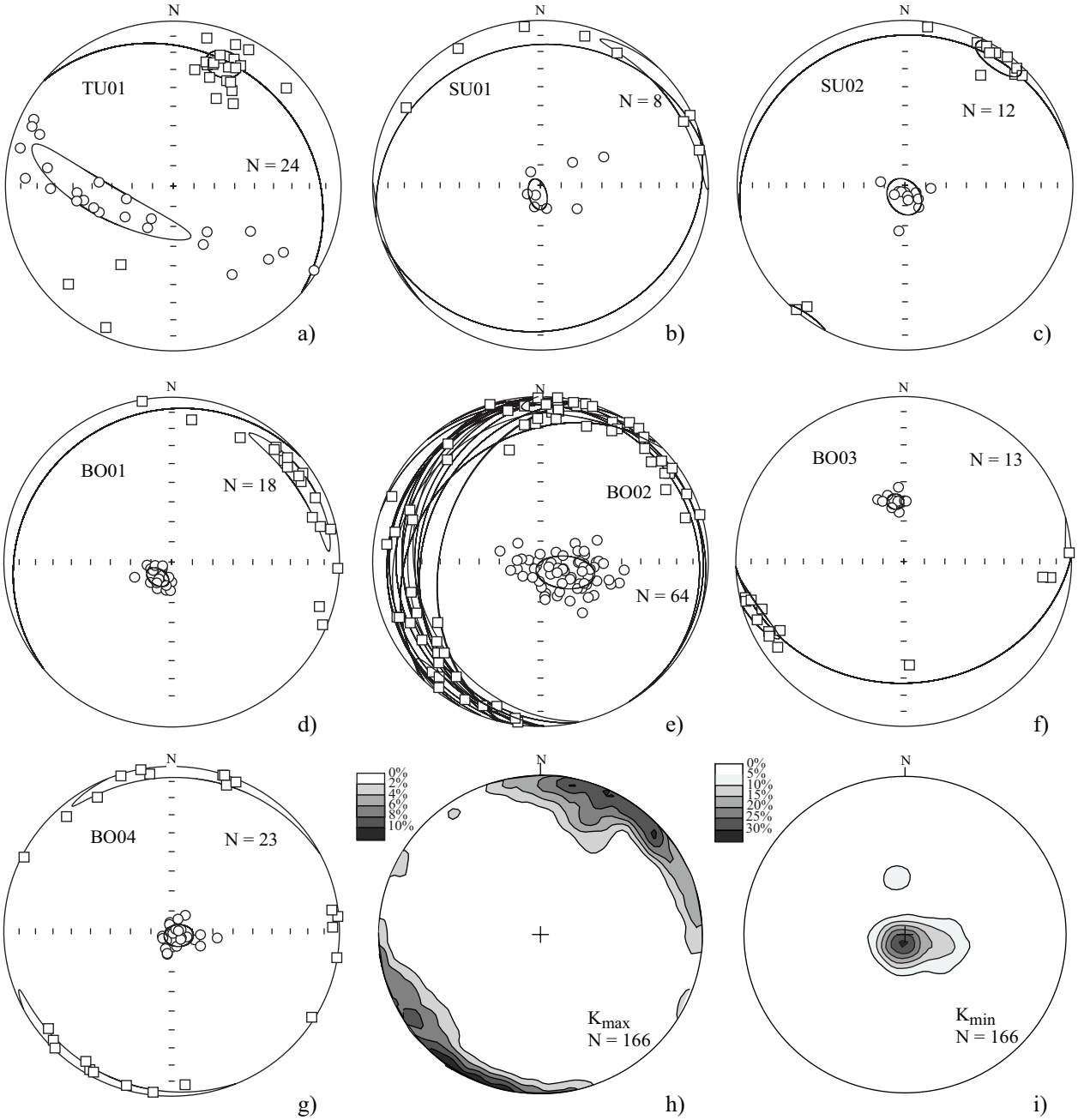


**Figure 3.** Mean magnetic susceptibility directions for samples analyzed in this study. (a)–(g) AMS plots with data plotted on lower hemisphere, equal-area projections, in geographic coordinates. Squares and circles represent maximum and minimum axes, respectively. Bedding planes (when detectable) are also represented. (h), (i) Contouring plots of $K_{min}$ (pole to magnetic foliation) and $K_{max}$ (magnetic lineation), respectively.

isolated between 280 and 630–670 °C (Figures 5f and 5h) or at 10–100 mT (Figure 5g).

Site-mean paleomagnetic directions are illustrated in Figures 6a–6g and listed in Table 2. All the sites have a well-defined mean direction with $\alpha_{95} < 11.3°$. Sites BO01, BO02, BO03, and TU01 have normal polarity, whereas sites SU01 and SU02 show reversed polarity. In geographic coordinates, all the sites have a mean direction distinct from the geocentric axial dipole (GAD) magnetic field direction (D/I = 0/56.5° and D/I = 180/-56.5° for normal and reversed directions, respectively), which suggests that they have not undergone recent overprint. At site BO02, both normal and reversed polarities were observed. Data from this section do not pass the bootstrap reversal test

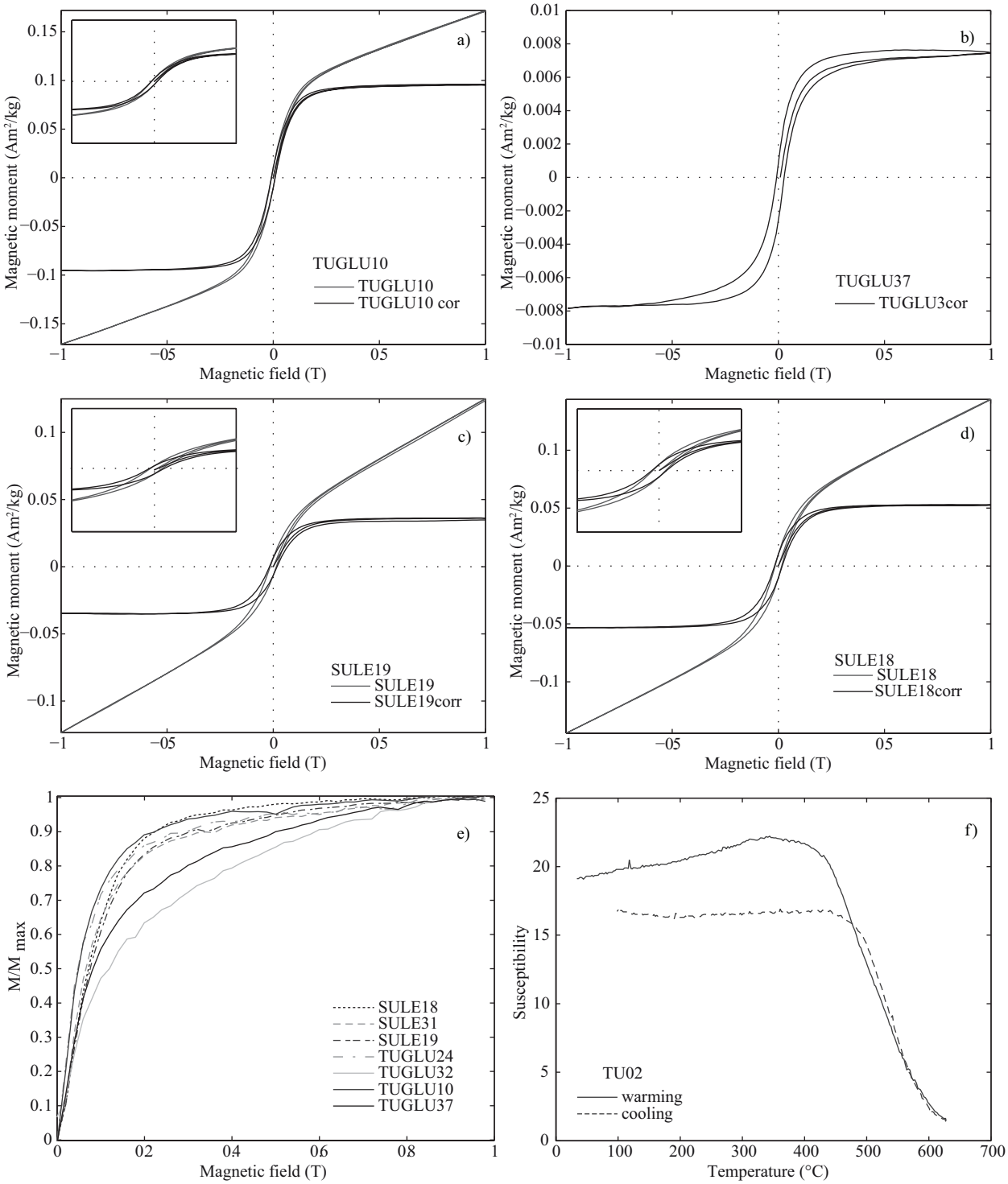


**Figure 4.** Magnetic mineralogy analysis of the analyzed sediments from the Çankırı Basin. (a)–(d) Hysteresis loops for representative samples. Gray curves represent the hysteresis loops before paramagnetic correction. (e) IRM acquisition curves showing the presence of both low-coercivity and high-coercitivity minerals in the analyzed samples. (f) Thermal susceptibility curve for TU02 specimens. Solid (dashed) line corresponds to the measure on warming (cooling).

(Tauxe *et al.* 1991), indicating that normal and reverse polarities are not antipodal (Table 2). We interpret this to be due to a viscous component acquired during a more recent period superimposed onto the normal polarity

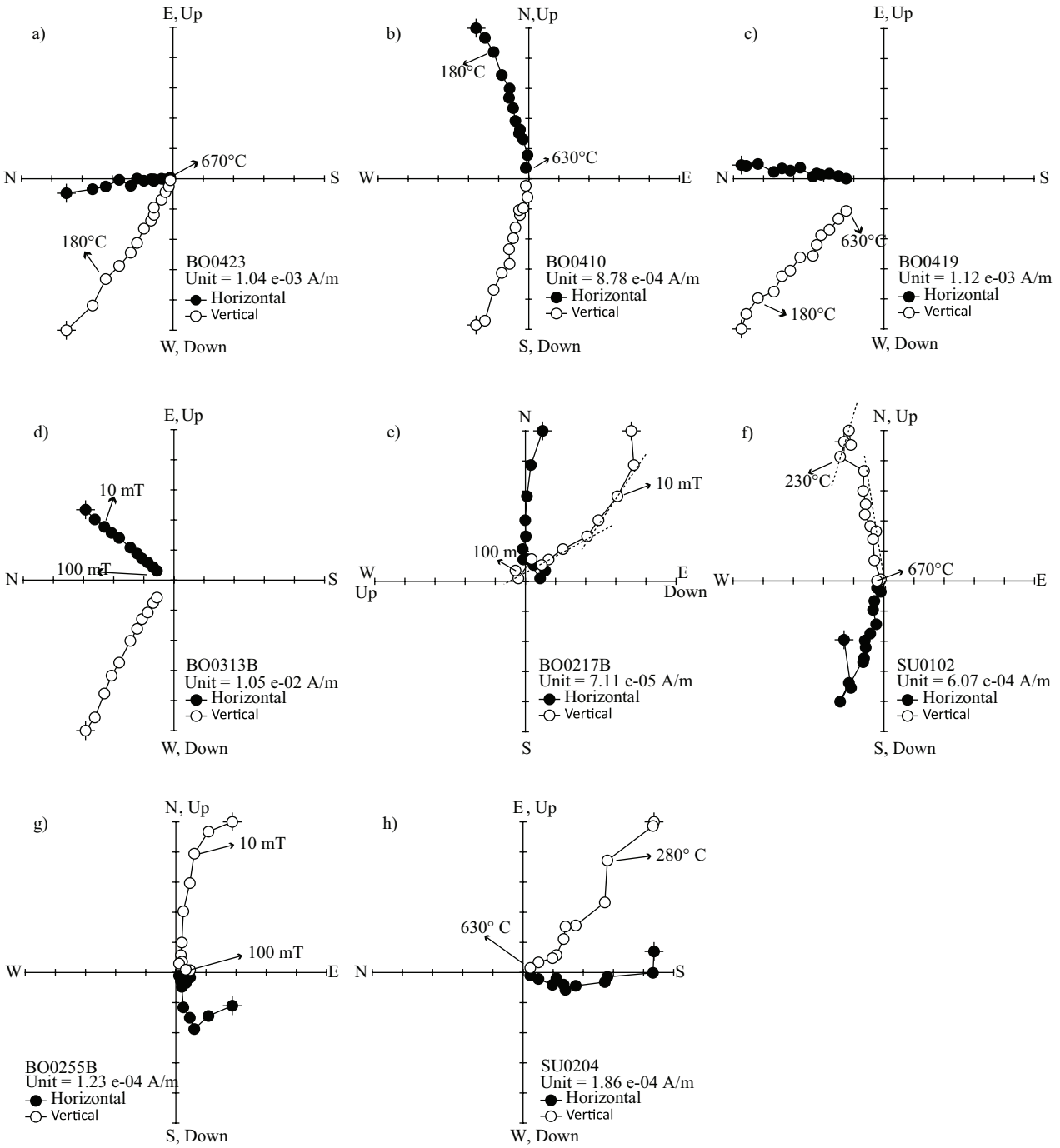


**Figure 5.** Vector component diagrams (Zijderveld diagrams, in geographic coordinates) for the progressive thermal and AF demagnetization of representative samples (demagnetization step values are in °C and mT, respectively). Empty and solid symbols represent projection on the vertical and horizontal planes, respectively.

directions, which has not been possible to isolate. For this reason, we do not include the normal polarity samples in the calculation of the mean direction for site BO02. When all sites are considered together, mean paleomagnetic direction from the basin is better grouped after bedding correction (Dec. = 3.4°, Inc. = 52.4°, k = 24.76, $\alpha_{95}$ = 12.4°) than before bedding correction (Dec. = 6.3°, Inc. = 56.8°, k = 21.31, $\alpha_{95}$ = 13.4°) (Figure 6h). These results, together with the presence of both normal and reversed polarity sites, permit consideration of the ChRM

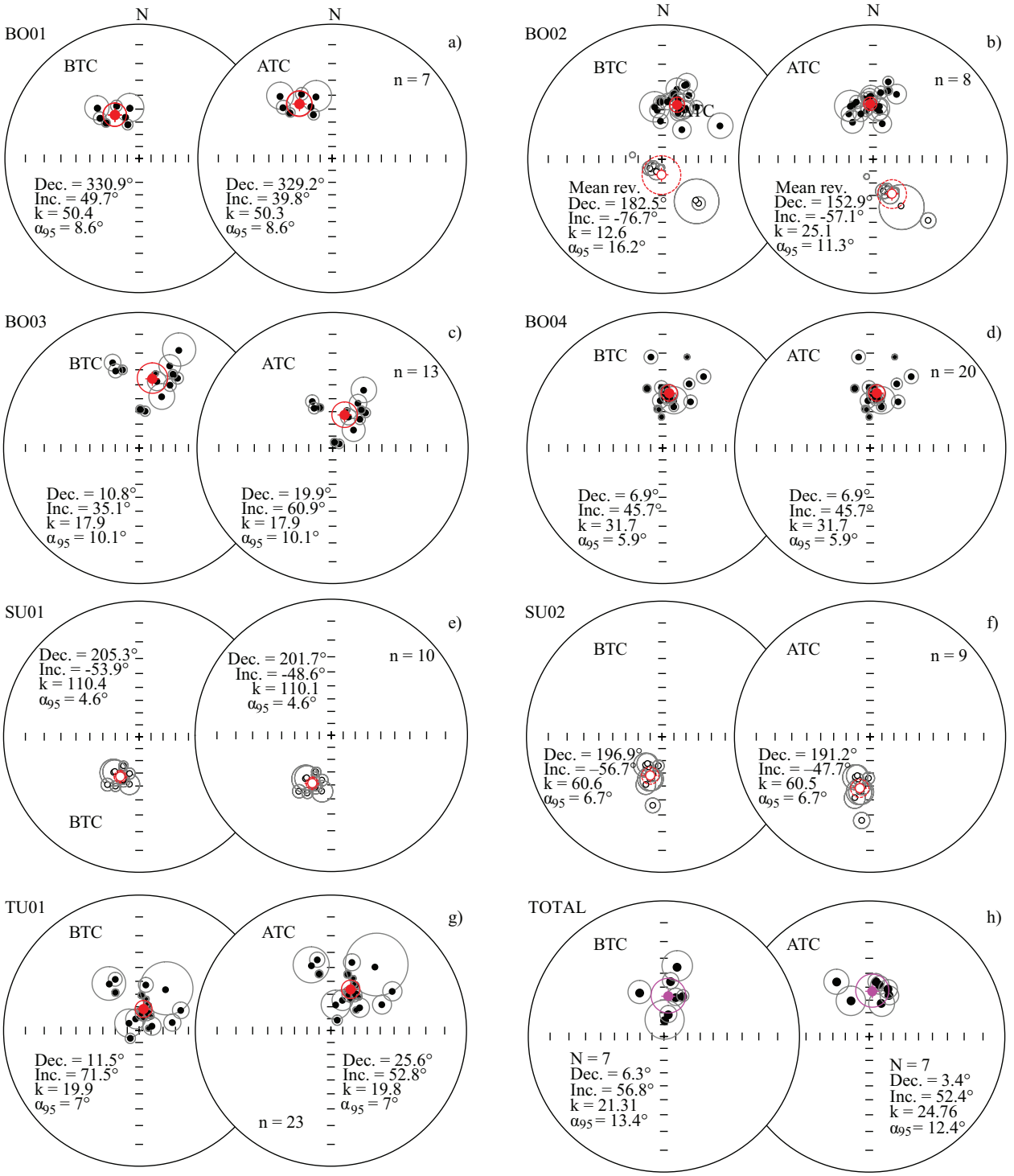


**Figure 6.** (a)–(g) Equal-area projection of the site-mean directions (red circles) from the Çankırı Basin; (h) Çankırı Basin-mean direction (violet circle). White and black symbols represent projection onto upper and lower hemisphere, respectively. Ellipses are projections of the $\alpha_{95}$ cone about the mean directions. BTC and ATC indicate data before and after tectonic correction.

magnetic components isolated in the Çankırı Basin as a primary magnetization, and therefore suitable for tectonic interpretation. Eurasia is not believed to have significantly rotated during the last 10 Ma (Besse & Coutillot 2002). For this reason, as reference direction we adopt the GAD field direction (in both normal and reversed polarity states),

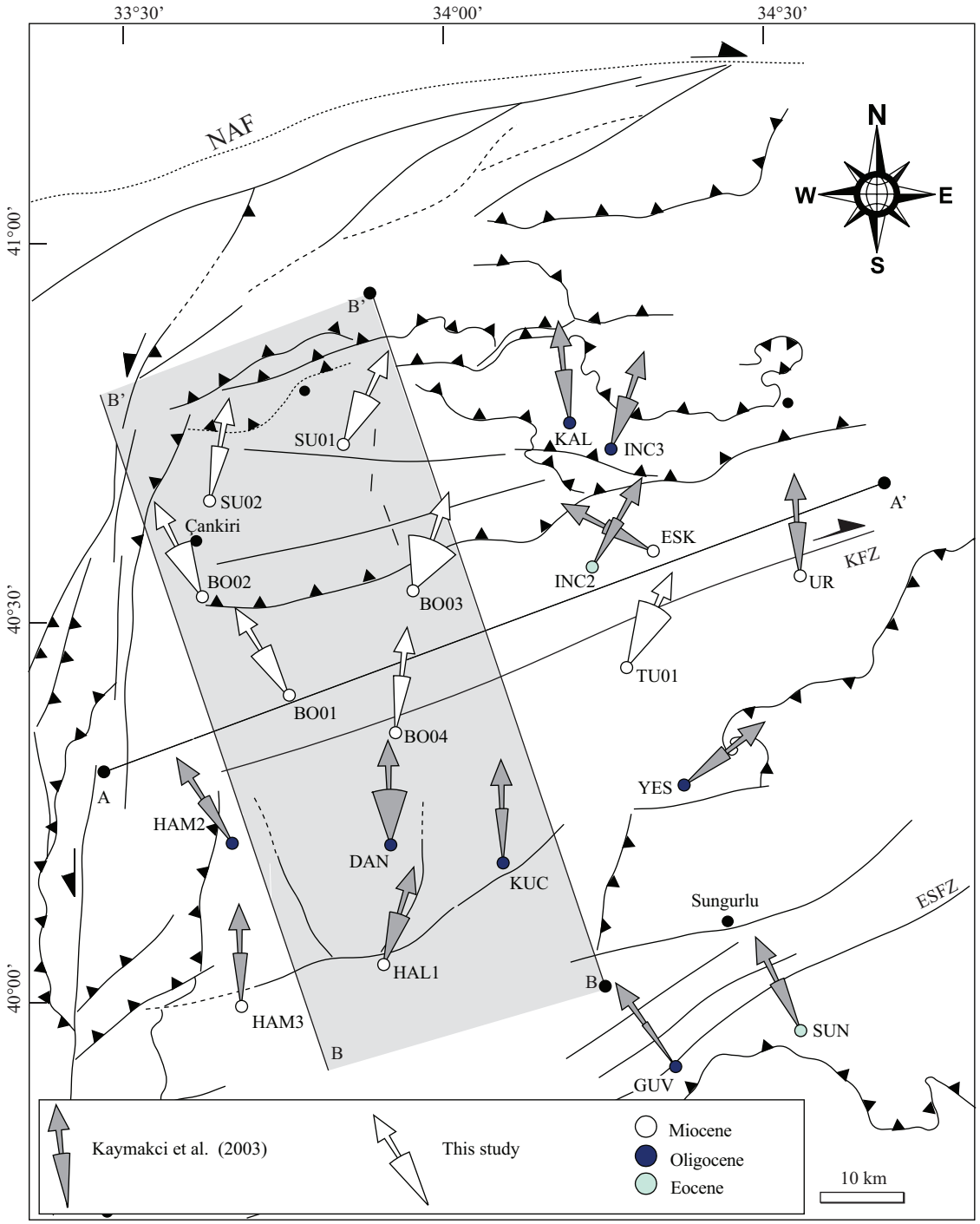


**Figure 7.** Paleomagnetic declinations (and relative confidence limits) from this study and from Kaymakçı *et al.* (2003). A-A' and B-B' (gray area) represent the 2 traces along which paleomagnetic rotation distribution was evaluated (see Figure 8).

assuming a negligible difference between Tortonian and present times. The resulting paleomagnetic rotations are reported in Figure 7 and Table 2, together with previous results from Çankırı Basin published by Kaymakçı *et al.* (2003), and will be discussed in the following section.

## 5. Discussion

Analysis of AMS can be used to establish the sedimentary and tectonic history in weakly deformed sediments (Tarling & Hrouda 1993). In the last 50 years, numerous studies have shown that AMS can be related to mineral and

**Table 2.** Paleomagnetic directions in the Çankırı Basin.

| Site | n/N | Age | $S_0$ | $D_{BTC}$ | $I_{BTC}$ | k | $\alpha_{95}$ | $D_{ATC}$ | $I_{ATC}$ | k | $\alpha_{95}$ | Rot (°) | Err (°) |
|---|---|---|---|---|---|---|---|---|---|---|---|---|---|
| BO01 | 7/18 | Upp. Miocene | 320, 10 | 330.9 | 49.7 | 50.4 | 8.6 | 329.2 | 39.8 | 50.3 | 8.6 | –30.8 | 11 |
| BO02_n* | 21/64 | Upp. Miocene | Variable | 15.7 | 44.7 | 34.8 | 5.5 | 356.9 | 45.7 | 44.1 | 4.8 | –3.1 | 7 |
| BO02_r | 8/64 | Upp. Miocene | Variable | 182.5 | –76.7 | 12.6 | 16.2 | 152.9 | –57.1 | 25.1 | 11.3 | –26.1 | 21 |
| BO03 | 13/13 | Upp. Miocene | 178, 27 | 10.8 | 35.1 | 17.9 | 10.1 | 19.9 | 60.9 | 17.9 | 10.1 | 19.9 | 21 |
| BO04 | 20/23 | Upp. Miocene | Sub-hor. | 6.9 | 45.7 | 31.7 | 5.9 | 6.9 | 45.7 | 31.7 | 5.9 | 6.9 | 8 |
| SU01 | 8/8 | Upp. Miocene | Variable | 205.3 | –53.9 | 110.4 | 4.6 | 201.7 | –48.6 | 110 | 4.6 | 25.8 | 22 |
| SU02 | 9/12 | Upp. Miocene | 348°, 10° | 196.9 | –56.7 | 60.6 | 6.7 | 191.2 | –47.7 | 60.5 | 6.7 | 11.2 | 10 |
| TU01 | 23/24 | Upp. Miocene | 40°, 20° | 11.5 | 71.5 | 19.9 | 7 | 25.6 | 52.8 | 19.8 | 7 | 25.6 | 12 |
| UR | 6/? | Upp. Miocene | ? | 353.1 | 34.9 | 58.8 | 8.8 | 356.5 | 43.9 | 58.8 | 8.8 | –3.5 | 12 |
| ESK | 7/? | Upp. Miocene | ? | 296.9 | 37.8 | 60.4 | 7.8 | 297.4 | 39.2 | 60.4 | **7.8** | –62.6 | 10 |
| KUC | 7/? | Mid. Miocene | ? | 161.8 | –56.2 | 102.4 | 6.0 | 178.5 | –59.8 | 102.4 | **6** | –1.5 | 12 |
| HAL1 | 5/? | Mid. Miocene | ? | 198.5 | 6.1 | 55.3 | 10.4 | 196.9 | –21.8 | 55.3 | **10.4** | 16.9 | 18 |
| KAL | 6/? | Oligocene | ? | 357 | 12.5 | 88.3 | 7.5 | 353.5 | 33 | 88.3 | **7.2** | –6.5 | 9 |
| YES | 6/? | Oligocene | ? | 53.8 | –17.9 | 83.5 | 7.4 | 51.6 | 22.2 | 83.5 | **7.4** | 51.6 | 8 |
| DAN | 5/? | Oligocene | ? | 347.9 | 37.6 | 20.4 | 17.3 | 356.3 | 29.2 | 20.4 | **17.3** | -3.7 | 20 |
| GUV | 7/? | Oligocene | ? | 120.9 | –45.8 | 378.8 | 3.1 | 144.1 | –35.6 | 378.8 | **3.1** | –35.6 | 3,8 |
| HAM3 | 5/? | Oligocene | ? | 184.8 | –44.8 | 103.9 | 7.5 | 178.1 | –28.1 | 103.9 | **7.5** | –1.9 | 8 |
| INC3 | 7/? | Oligocene | ? | 15.6 | 19.7 | 35.4 | 10.3 | 18.6 | 44.3 | 35.4 | **10.3** | 18.6 | 14 |
| HAM2 | 7/? | Oligocene | ? | 331.7 | 15.7 | 72.4 | 7.1 | 326.6 | 14.4 | 72.4 | **7.1** | –33.4 | 7 |
| SUN | 8/? | Eocene | ? | 153.1 | 16.4 | 51.8 | 7.8 | 152.9 | –12.6 | 51.8 | **7.8** | –27.1 | 8 |
| INC2 | 4/? | Eocene | ? | 207.3 | 20 | 187.1 | 6.7 | 208.7 | –12.5 | 187.1 | **6.7** | 28.7 | 7 |

n/N = number of stable directions/total number of demagnetized samples at each site; D, I = site-mean declinations and inclinations calculated before ($D_{BTC}$, $I_{BTC}$) and after ($D_{ATC}$, $I_{ATC}$) tectonic correction; k and $\alpha_{95}$ = statistical parameters after Fisher (1953); $S_0$ = bedding attitude (azimuth of the dip and dip values). Sites with asterisk have been discarded because of magnetic overprint; ? refers to missing information from original paper of Kaymakçı *et al.* 2003.

tectonic fabrics and that it can be successfully employed in the field of structural geology as a powerful tool for fabric analysis in different rock types (e.g., Graham 1954; Goldstein 1980; Kligfield *et al.* 1983; Housen & Van der Pluijm 1991; Tarling & Hrouda 1993; Borradaile & Henry 1997; Porreca *et al.* 2003; Cifelli *et al.* 2005; Porreca *et al.* 2006; Archanjo *et al.* 2008; Debacker *et al.* 2009; Cifelli *et al.* 2012). The AMS fabric has distinctive character in extensional and compressional tectonic settings, and for this reason the orientation of $K_{max}$ (magnetic lineation) represents a useful structural parameter for integration with the classic strain markers in order to define the deformation pattern, especially in sedimentary sequences (Mattei *et al.* 1997; Cifelli *et al.* 2004, 2007). In particular, in weakly deformed fine-grained sediments, such as those analyzed in this work, where deformation is poorly developed or absent at the outcrop scale, AMS may be used to reconstruct the deformation pattern of sediments (Kissel *et al.* 1986; Lee *et al.* 1990; Parès 2002; Cifelli *et al.* 2005, 2009). AMS data from the Çankırı Basin show a magnetic foliation subparallel to the bedding (Figure 3h), which suggests a primary sedimentary magnetic fabric (e.g., Graham 1966; Kissel *et al.* 1986; Lee *et al.* 1990; Sagnotti & Speranza 1993; Scheepers & Langereis 1994; Mattei *et al.* 1999). Magnetic lineations show 2 main trends: WSW-ENE in the central part of the basin and NNE-SSW in the western and eastern basin edges (Figure 3i). Such magnetic lineations in sedimentary rocks can be of depositional (related to depositional currents) or of tectonic origin. However, at all sites measured in this study, the trend of the magnetic lineation is maintained through sequences that differ in sedimentological characters and age. Furthermore, the distribution of magnetic lineation directions parallels the trend of thrust faults along the Ω-shaped tectonic boundary of the basin. All of these observations support a tectonic origin of the magnetic lineation in the Çankırı Basin.

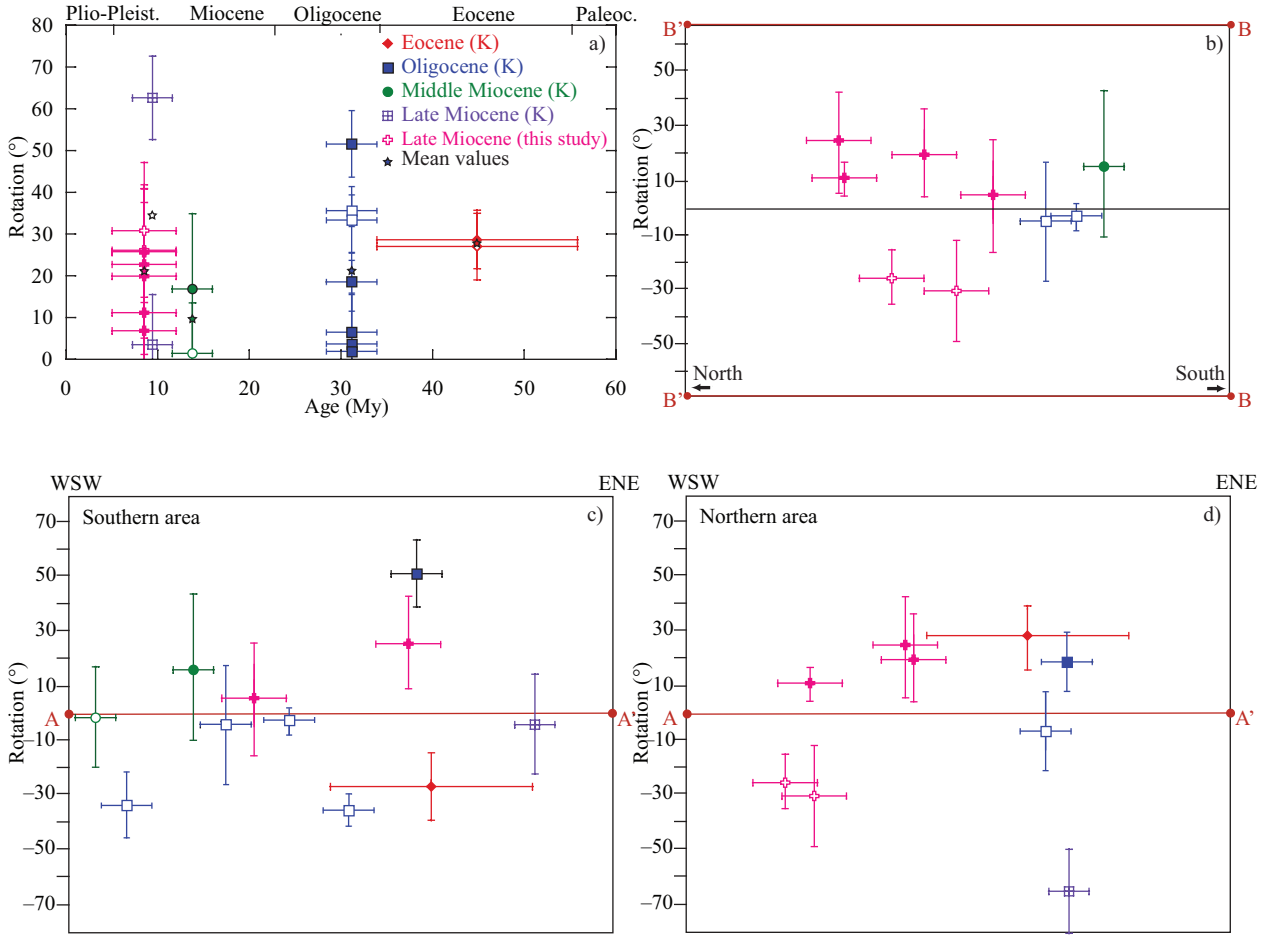


**Figure 8.** (a) Site-mean rotations (in degrees) versus age for paleomagnetic rotations in the Çankırı Basin; (b) site mean rotations (in degrees) distribution along a NNW-SSW transect (trace is shown in Figure 7); (c), (d) site-mean rotation (in degrees) distribution along a WSW-ESE profile (trace is shown in Figure 7) in the southern and northern sector of the basin, respectively.

Based on paleomagnetic and structural evidences, Kaymakçı *et al.* (2003) proposed an indentation model to explain the tectonic evolution and Ω-shape of the Çankırı Basin. Due to the irregular nature of the indenting Kırşehir Block in its northern part, intense deformation resulted both within the Sakarya continent and in the infill of the Çankırı Basin. This resulted in thrusting and strike-slip faulting, which caused the rotation of the rims of the Çankırı Basin and the acquisition of its characteristic Ω-shape. According to this model, counterclockwise rotations should have occurred in the western margin of the basin and clockwise rotations in the eastern sector during Eocene and Oligocene times, whereas during the Miocene no significant rotations should be expected in the basin. Our paleomagnetic data come from Miocene sedimentary sequences outcropping in the northern and central part of the basin. These data add to those published by Kaymakçı *et al.* (2003), both in terms of age and geographic distribution, and they increase the paleomagnetic dataset available for constraining the tectonic evolution of the Çankırı Basin. The collective pattern of paleomagnetic rotations is shown in Figure 7 and in Table 2. In the following discussion, we evaluate these results in terms of geographic and age distribution of the paleomagnetic rotations to test the reliability of the indentation model proposed by Kaymakçı *et al.* (2003).

The age distribution of paleomagnetic rotations is shown in Figure 8a. In this diagram, we report the amount of paleomagnetic rotations (indicated by the modulus of rotation, without any distinction between CW and CCW rotations) versus the age of the sampled sites. The mean rotation values calculated for Eocene, Oligocene, and Miocene sites provide no evidence for any progressive decrease in the amount of paleomagnetic rotations between Eocene and Miocene times. In fact, when all the data are considered together, the mean rotations for Eocene and Late Miocene sites are 28° and 22°, respectively, which indicates that significant paleomagnetic rotations occurred

after Late Miocene times. In the model of Kaymakçı *et al.* (2003), the indentation started before Eocene and ended before Miocene times. However, our results indicate that the deformation processes were still active at the end of the Late Miocene and imply that the timing of the tectonic processes in this area requires revision.

The geographic distribution of the paleomagnetic rotations is also evaluated along 2 different profiles. The first is NNW-SSE oriented (Figure 8b), whereas the second is WSW-ENE oriented (Figures 8c and 8d). In the NNW-SSW profile, large paleomagnetic rotations have been observed in almost all the sites (the ones included in the gray area in Figure 7) from the central and northern sector of the basin, whereas no paleomagnetic rotations have been measured in most of the sites from the southern part of the basin, with the exception of those sites located close to the western and eastern margins (not included in the Figure). In the southern profile (Figure 8c), 2 different sectors can be observed. These comprise: 1) the central part of the basin, where no significant paleomagnetic rotations have been measured, and 2) the western and the eastern tectonic margins, with each characterized by opposite tectonic rotations within very narrow areas. Conversely, in the northern transect (Figure 8d), significant paleomagnetic rotations have been observed at almost all the sites, indicating that in this portion of the basin, tectonic rotations have been more important compared to the southern part. These paleomagnetic data suggest an alternative model for the tectonic evolution of the Çankırı Basin since the late Miocene.

Along the ENE-WSW–oriented northern margin of the basin, clockwise paleomagnetic rotations have been measured in most of the paleomagnetic sites (Figure 7). This margin developed parallel to the main strand of the right-lateral North Anatolian Fault (NAF), suggesting that the measured CW rotations could be due to localized deformation related to a post-Late Miocene right-lateral reactivation of this basin tectonic boundary. At the same time, counterclockwise rotations, measured along the N-S–oriented western margin of the basin, appear to be related to a left-lateral motion of the main tectonic elements, which form the basin margin in this area. These observations suggest that, since the Late Miocene, paleomagnetic rotations in the Çankırı Basin have been mainly controlled by strike-slip motions along the basin margin, probably connected with the formation and activity of the NAF. Moreover, paleomagnetic rotations do not seem to be related to the indentation of the Kırşehir Block against the Sakarya continent, which resulted in the Ω-shape of the Çankırı Basin. In fact, the large curvature of the tectonic structures that define the margins of the basin does not correspond to large, opposite, paleomagnetic rotations within the basin. One possible explanation could be that the Çankırı Basin, located in the thrust footwall, was not involved in major paleomagnetic rotations (Figure 6h); during the indentation process these could have been concentrated along the hanging wall of the ophiolitic thrusts that form the main tectonic boundary of the basin.

## 6. Conclusion

Paleomagnetic data from the Çankırı Basin show that the timing and geographic distribution of tectonic rotations are not compatible with the indentation model proposed by Kaymakçı *et al.* (2003). In fact, the distribution of tectonic rotations is not symmetrical within the basin and they also influenced Late Miocene continental sediments, and they are therefore younger than originally supposed by Kaymakçı *et al.* (2003). Furthermore, paleomagnetic rotations appear to increase from the southern portion of the basin toward the north and from the central part toward the basin margins. This geographic and age distribution can be reasonably explained in terms of post-Late Miocene reactivation of the Çankırı Basin margins, possibly related to the activity on the right-lateral North Anatolian strike-slip fault. With this tectonic interpretation, the complex pattern of paleomagnetic rotations appears to be connected with a local block-rotation mechanism due to the activity of faults with the strike-slip component of motion along the tectonic margins of the Çankırı Basin.

## Acknowledgments

The authors would like to thank Subject Editor Attila Çiner for his support. The authors are also grateful to Paolo Ballato, John Piper, and Fabio Speranza for their constructive reviews. Peter Joniak, Marianna Kovacova, Ilaria Mazzini, and Tamas Mikes are warmly thanked for participating and helping in the paleomagnetic sampling. This work is part of the Vertical Anatolian Movements Project (VAMP), funded by the TOPOEUROPE initiative of the European Science Foundation, including contributions by the Istituto di Geologia Ambientale e Geoingegneria del Consiglio Nazionale delle Ricerche (IGAG-CNR) (com. TA.P05.009, mod. TA.P05.009.003) and TUBİTAK Project: 107Y333.

## References

Archanjo, C.J., Hollanda, M.H.B.M., Rodrigues, S.W.O., Neves, B.B.B. & Armstrong, R. 2008. Fabrics of pre- and syntectonic granite plutons and chronology of shear zones in the Eastern Borborema Province, NE Brazil. *Journal of Structural Geology* **30**, 310–326.

Besse, J. & Courtillot, V. 2002. Apparent and true polar wander and the geometry of the geomagnetic field over the last 200 Myr. *Journal of Geophysical Research* **107**, doi:10.1029/2000JB000050.

Borradaile, G.J. & Henry, B. 1997. Tectonic applications of magnetic susceptibility and its anisotropy. *Earth Science Reviews* **42**, 49–93.

Chadima, M. & JELINEK, V. 2009. AniSoft 42 Software, Anisotropy Data Browser for Windows. Brno, Czech Republic.

Cifelli, F., Mattei, M., Chadima, M., Hirt, A. & Hansen, A. 2005. The origin of tectonic lineation in extensional basins: combined neutron texture and magnetic analyses on "undeformed" clays. *Earth and Planetary Science Letters* **235**, 62–78.

Cifelli, F., Mattei, M., Chadima, M., Lenser, S. & Hirt, A.M. 2009. The magnetic fabric in "undeformed clays": AMS and neutron texture analyses from the Rif Chain (Morocco). *Tectonophysics* **466**, 79–88.

Cifelli, F., Minelli, L., Rossetti, F., Urru, G. & Mattei, M. 2012. The emplacement of the Late Miocene Monte Capanne intrusion (Elba Island, Central Italy): constraints from magnetic fabric analyses. *International Journal of Earth Sciences* **101**, 787–802.

Cifelli, F., Rossetti, F. & Mattei, M. 2007. The architecture of brittle postorogenic extension: results from an integrated structural and paleomagnetic study in north Calabria (southern Italy). *Geological Society of America Bulletin* **119**, 221–239.

Cifelli, F., Rossetti, F., Mattei, M., Hirt, A.M., Funiciello, R. & Tortorici, L. 2004. An AMS, structural and paleomagnetic study of Quaternary deformation in eastern Sicily. *Journal of Structural Geology* **26**, 29–46.

Debacker, T.N., Hirt, A.M., Sintubin, M. & Robion, P. 2009. Differences between magnetic and mineral fabrics in low-grade, cleaved siliciclastic pelites: a case study from the Anglo-Brabant Deformation Belt (Belgium). *Tectonophysics* **466**, 32–46.

Evans, I. & Hall, S.A. 1990. Paleomagnetic constraints on the tectonic evolution of the Sakarya Continent, northwestern Anatolia. *Tectonophysics* **182**, 357–372.

Fisher, R. 1953. Dispersion on a sphere. *Proceedings of the Royal Society of London Series A* **217**, 295–305.

Gansser, A. 1974. The ophiolitic mélange, a world-wide problem on Tethyan examples. *Eclogae Geologicae Helvetiae* **67**, 479–507.

Goldstein, A.G. 1980. Magnetic susceptibility anisotropy of mylonites from the Lake Char mylonite zone, southeastern New England. *Tectonophysics* **66**, 197–211.

Görür, N., Tüysüz, O. & Şengör, A.M.C. 1998. Tectonic evolution of the Central Anatolian Basins. *International Geology Review* **40**, 831–850.

Graham, J.W. 1954. Magnetic susceptibility anisotropy, an unexploited petrofabric element. *Geological Society of America Bulletin* **65**, 1257–1258.

Graham, J.W. 1966. *Significance of Magnetic Anisotropy in Appalachian Sedimentary Rocks.* American Geophysical Union Geophysics Publications, Monograph 10.

Gürsoy, H., Piper, J.D.A., Tatar, O. & Temiz, H. 1997. A palaeomagnetic study of the Sivas Basin, central Turkey: crustal deformation during lateral extrusion of the Anatolian Block. *Tectonophysics* **271**, 89–105.

Housen, B.A. & van der Pluijm, B. 1991. Slaty cleavage development and magnetic anisotropy fabrics. *Journal of Geophysical Research* **96**, 9937–9946.

Hrouda, F. 1982. Magnetic anisotropy of rocks and its application in geology and geophysics. *Surveys in Geophysics* **5**, 37–82.

Jelínek, V. 1981. Characterization of the magnetic fabric of rocks. *Tectonophysics* **79**, 63–67.

Kaymakçı, N., 2000. *Tectono-Stratigraphical Evolution of the Çankırı Basin (Central Anatolia, Turkey)*. PhD, Universiteit Utrecht, Utrecht, the Netherlands.

Kaymakçı, N., Duermeijer, C.E., Langereis, C., White, S.H. & VAN DIJK, P.M. 2003. Palaeomagnetic evolution of the Çankırı Basin (central Anatolia, Turkey): implications for oroclinal bending due to indentation. *Geological Magazine* **140**, 343–355.

Kaymakçı, N., Ozcelik, Y., White, S.H. & Van dijk, P.M. 2009. Tectono-stratigraphy of the Çankırı Basin: Late Cretaceous to early Miocene evolution of the Neotethyan Suture Zone in Turkey: *Geological Society, London, Special Publications* **311**, 67–106.

Kirschvink, J.L. 1980. The least-squares line and plane and the analysis of palaeomagnetic data. *Geophysical Journal of the Royal Astronomical Society* **62**, 699–718.

Kissel, C., Barrier, E., Laj, C. & Lee, T.Q. 1986. Magnetic fabric in "undeformed" marine clays from compressional zones. *Tectonics* **5**, 769–781.

Kligfield, R., Lowrie, W., Hirt, A. & Siddans, A.W.B. 1983. Effect of progressive deformation on remanent magnetization of Permian redbeds from the Alpes Maritimes (France). *Tectonophysics* **98**, 59–85.

Lee, T.Q., Kissel, C., Laj, C., Horng, C.S. & Lue, Y.T. 1990. Magnetic fabric analysis of the Plio Pleistocene sedimentary formations of the coastal range of Taiwan. *Earth and Planetary Science Letters* **98**, 23–32.

Mattei, M., Sagnotti, L., Faccenna, C. & Funiciello, R. 1997. Magnetic fabric of weakly deformed clay-rich sediments in the Italian peninsula: relationship with compressional and extensional tectonics. *Tectonophysics* **271**, 107–122.

Mattei, M., Speranza, F., Argentieri, A., Rossetti, F., Sagnotti, L. & Funiciello, R. 1999. Extensional tectonics in the Amantea basin (Calabria, Italy): a comparison between structural and magnetic anisotropy data. *Tectonophysics* **307**, 33–49.

Meijers, M.J.M., Kaymakçı, N., van Hinsbergen, D.J.J., Langereis, C.G., Stephenson, R.A. & Hippolyte, J.C. 2010. Late Cretaceous to Paleocene oroclinal bending in the central Pontides, Turkey. *Tectonics* **29**, TC4016.

Michel, G.W., Waldhor, M., Neugebauer, J. & Appel, E. 1995. Sequential rotation of stretching axes and block rotations: a structural and paleomagnetic study along the North Anatolian Fault. *Tectonophysics* **243**, 97–118.

Morris, A. & Robertson, A.H.F. 1993. Miocene remagnetisation of carbonate platform and Antalya Complex units within the Isparta angle, SW Turkey. *Tectonophysics* **220**, 243–266.

Parès, J. 2002. Evaluating magnetic lineations (AMS) in deformed rocks. *Tectonophysics* **350**, 283–298.

Piper, J.D.A., Moore, J.M., Tatar, O., Gursoy, H. & Park, R.G. 1996. Palaeomagnetic study of crustal deformation across an intracontinental transform: the North Anatolian Fault Zone in Northern Turkey. *Geological Society, London, Special Publications* **105**, 299–310.

Piper, J.D.A., Tatar, O. & Gürsoy, H. 1997. Deformational behaviour of continental lithosphere deduced from block rotations across the North Anatolian fault zone in Turkey. *Earth and Planetary Science Letters* **150**, 191–203.

Piper, J.D.A., Gursoy, H., Tatar, O., Beck, M.E., Rao, A., Kocbulut, F. & Mesci, B.L. 2010. Distributed neotectonic deformation in the Anatolides of Turkey: a palaeomagnetic analysis. *Tectonophysics* **488**, 31–50.

Platzman, E.S., Platt, J.P., Tapirdamaz, C., Sanver, M. & Rundle, C.C. 1994. Why are there no clockwise rotations along the North Anatolian Fault Zone? *Journal of Geophysical Research* **99**, 21705–21715.

Platzman, E.S., Tapirdamaz, C. & Sanver, M. 1998. Neogene anticlockwise rotation of central Anatolia (Turkey): preliminary palaeomagnetic and geochronological results. *Tectonophysics* **299**, 175–189.

Porreca, M., Acocella, V., Massimi, E., Mattei, M., Funiciello, R. & De Benedetti, A.A. 2006. Geometric and kinematic features of the dike complex at Mt. Somma, Vesuvio (Italy). *Earth and Planetary Science Letters* **245**, 389–407.

Porreca, M., Mattei, M., Giordano, G., De Rita, D. & Funiciello, R. 2003. Magnetic fabric and implications for pyroclastic flow and lahar emplacement, Albano maar, Italy. *J. Geophys. Res.* **108**, 2264.

Rojay, B. 1995. Post-Triassic evolution of Central Pontides: Evidence from Amasya region, Northern Anatolia. *Geologica Romana* **31**, 329–350

Rojay, B., Altıner, D., Altıner, S.O., Önen, P., James, S.L. & Thirlwall, M.F. 2004. Geodynamic significance of the Cretaceous pillow basalts from North Anatolian Ophiolitic Mélange Belt, Central Anatolia, Turkey: geochemical and paleontological constraints. *Geodinamica Acta* **17**, 349–361.

Sagnotti, L. & Speranza, F. 1993. Magnetic fabric analysis of the Plio-Pleistocene clayey units of the Sant'Arcangelo basin, southern Italy. *Physics of the Earth and Planetary Interiors* **77**, 165–176.

Sanver, M. & Ponat, E. 1981. Kırşehir ve dolaylarına ilişkin paleomagnetik bulgular. Kırşehir masifinin rotasyonu. *Istanbul Yerbilimleri* **2**, 2–8 (in Turkish with English abstract).

Saribudak, M., Sanver, M., Şengör, A.M.C. & Görür, N. 1990. Palaeomagnetic evidence for substantial rotation of the Almacik flake within the North Anatolian Fault zone, NW Turkey. *Geophysical Journal International* **102**, 563–568.

Scheepers, P.J.J. & Langereis, C.G. 1994. Magnetic fabric of the Pleistocene clays from the Tyrrhenian arc: a magnetic lineation induced in the final stage of the middle Pleistocene compressive event. *Tectonics* **13**, 1190–1200.

Şengör, A.M.C. 2003. The repeated rediscovery of mélanges and its implications for the possibility and role of objective evidence in the scientific enterprise. *Geological Society of America Special Paper* **373**, 385–445.

Şengör, A.M.C. & Yılmaz, Y. 1981. Tethyan evolution of Turkey: a plate tectonic approach. *Tectonophysics* **75**, 181–241.

Tarling, D.H. & Hrouda, F. 1993. *The Magnetic Anisotropy of Rocks*. Chapman & Hall, London.

Tatar, O., Piper, J.D.A., Park, R.G. & Gürsoy, H. 1995. Palaeomagnetic study of block rotations in the Niksar overlap region of the North Anatolian Fault Zone, central Turkey. *Tectonophysics* **244**, 251–266.

Tauxe, L., Kylstra, N. & Constable, C. 1991. Bootstrap statistics for paleomagnetic data. *Journal of Geophysical Research* **96**, 723–740.

Van Der Voo, R. 1968. Paleomagnetism and the Alpine tectonics of Eurasia IV: Jurassic, Cretaceous and Eocene pole positions from northeastern Turkey. *Tectonophysics* **6**, 251–269.